

Phase diagram and phase transitions of krypton on graphite in the one-to-two-layer regime

E. D. Specht, M. Sutton, and R. J. Birgeneau
*Department of Physics, Massachusetts Institute of Technology,
 Cambridge, Massachusetts 02139*

D. E. Moncton
Brookhaven National Laboratory, Upton, New York 11973

P. M. Horn
*IBM Thomas J. Watson Research Center,
 Yorktown Heights, New York 10598*

(Received 17 April 1984)

We report a high-resolution x-ray diffraction study of the freezing transitions of krypton on graphite for coverages above one monolayer. For pressure $P > 430$ Torr there is a single continuous incommensurate-fluid-to-incommensurate-solid freezing transition. For $P < 430$ Torr the freezing at fixed pressure is doubly reentrant with the succession of phases fluid \rightarrow commensurate solid \rightarrow reentrant fluid \rightarrow incommensurate solid. The first transition is of first order, whereas the other two are continuous within the experimental resolution.

The system, krypton on graphite, in the monolayer coverage range continues to be the subject of intensive experimental,¹⁻⁴ and theoretical study.⁵⁻⁷ The reason for this is that with quite small changes in coverage or temperature the krypton overlayer exhibits commensurate (C), incommensurate (IC), and fluid (F) phases. Further, a novel reentrant fluid (RF) phase separating the C and IC phases has been discovered.¹ In spite of the extensive research, the nature of the phase diagram and all of the phase transitions is still quite controversial.^{1,5-8} Indeed, neither the universality class and order of the various phase transitions, nor the phase diagram topology itself, is agreed upon.

In this Rapid Communication we report the salient results of a synchrotron x-ray study of the krypton phases and transitions for coverages above one monolayer. The experiments were carried out at the Stanford Synchrotron Radiation Laboratory (SSRL) using the wiggler beam line VII-2 as described in Ref. 9. Ge(111) monochromator and analyzer crystals provided a longitudinal resolution of 0.0005 \AA^{-1} half-width at half maximum (HWHM), much less than the intrinsic overlayer solid peak width of 0.0023 \AA^{-1} . For the substrate we used a sample of Union Carbide ZYX exfoliated graphite similar to those described previously.¹ The experimental techniques including the gas handling and cryogenics were closely similar to those described in Ref. 1.

We consider first the general phase diagram in the temperature interval of 114 to 130 K. As discussed previously,¹ the C, F, and RF phases give very different diffraction signatures so that the boundary between the commensurate and fluid phases may be readily determined. The RF-I boundary is somewhat more difficult to locate precisely but nevertheless may be reasonably estimated. The phase diagram so obtained is shown in Fig. 1. The corresponding coverages could not be determined in this experiment. However, from the work of Butler, Litzinger, and Stewart,³ the lower-pressure commensurate solid freezing at ~ 115 K corresponds to ~ 1.0 commensurate ($\sqrt{3} \times \sqrt{3} R 30^\circ$) monolayers, whereas the terminus of the commensurate solid re-

gion at ~ 430 Torr occurs at a coverage of ~ 1.5 monolayers. We will discuss the detailed nature of these various phases and the transitions between them below. Here we emphasize the important qualitative features. The most dramatic result is that there is no C-IC-F multicritical point at high temperatures.³ Instead the ordinary fluid phase F connects continuously onto a reentrant fluid which in turn evolves continuously with decreasing temperature into the modulated fluid previously observed at lower temperatures¹ (≤ 94 K). It appears that the transition identified as C-IC in the heat-capacity study³ is actually a C-RF transition. In addition, the heat-capacity peak observed at ~ 128 K above 430 Torr which was associated with an F-IC transition does not represent a phase transition but rather the rapid development of correlations near the terminus of the C phase. The heat-capacity peak associated with the F-IC transition, which, as we shall see below, is continuous, is

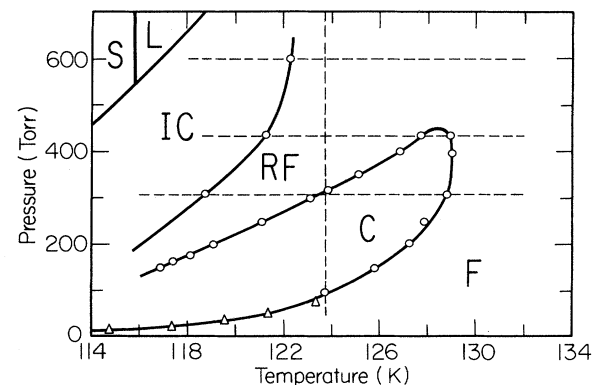


FIG. 1. Phase diagram of near-monolayer krypton: F: fluid, C: commensurate solid, RF: reentrant fluid, IC: incommensurate solid, S: bulk solid, L: bulk liquid. Triangles are from Ref. 4, circles this work. Scans were taken along the dashed lines.

unobservably weak. The unusual topology for the phase diagram can be understood qualitatively as follows. For coverages near two monolayers clearly the close-packed IC phase will be favored. However, for coverages closer to one monolayer, at high temperatures there will be significant occupation of the second layer. The second layer thus will form a dilute lattice gas while the structure of the depopulated first layer will be commensurate. As temperature is decreased condensation occurs into the first layer thence driving the commensurate-incommensurate transition. As demonstrated by Moncton *et al.*,¹ this C-IC transition is, in fact, a melting transition. This accounts for the reentrant character. Finally the RF freezes into an IC solid. Caflisch, Kardar, and Berker¹⁰ have proposed a similar model and by explicit renormalization-group calculations they have produced a phase diagram similar to Fig. 1. A model predicting reentrant melting has also been proposed by Dash and Muirhead¹¹ although their physical mechanisms does not involve a C-IT.

We now discuss the diffraction profiles in the various phases together with the details of the phase transitions. Figure 2 shows a series of scans at a fixed pressure of 310 Torr. Although not shown explicitly, data were collected from $Q = 1.2$ to 2.4 \AA^{-1} to determine accurately the wings of the scattering. We have subtracted background scattering due both to the graphite and to the krypton gas, as well as a weak bulk liquid signal centered at $\sim 1.85 \text{ \AA}^{-1}$ with a half-width of $\sim 0.2 \text{ \AA}^{-1}$ presumably due to capillary-condensed krypton.

The solid lines in the figure represent the powder aver-

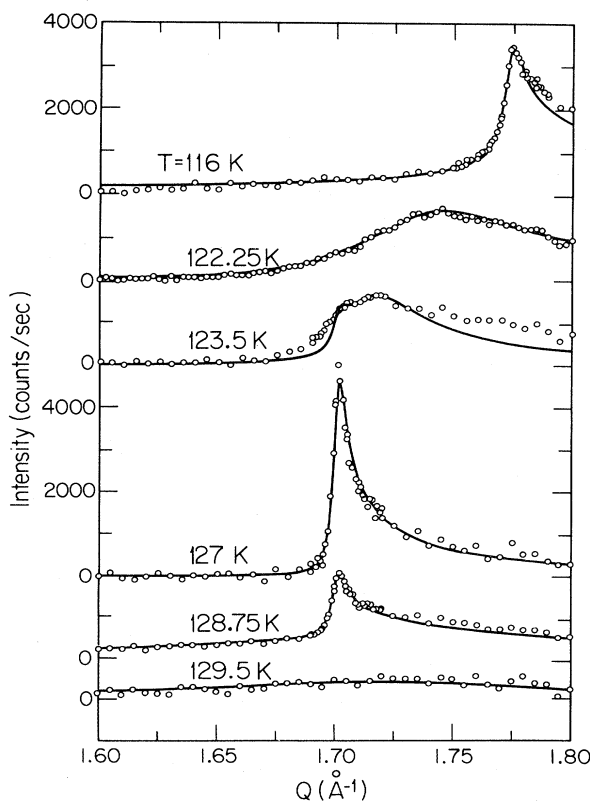


FIG. 2. Kr (10) diffraction profiles at $P=310$ Torr. Solid lines are model line shapes from Stephens *et al.* (Ref. 1) as discussed in the text.

aged two-dimensional (2D) line shapes as discussed by Stephens *et al.*¹ We begin our discussion at the highest temperature, 129.5 K. Here, there is very broad scattering which is well described by an intrinsic Lorentzian with half-width $\kappa=0.06 \text{ \AA}^{-1}$; the best-fit peak position is $Q_0=1.71 \pm 0.01 \text{ \AA}^{-1}$ close to the commensurate solid value of 1.70 \AA^{-1} . At 128.75 K there is, in addition to the broad fluid scattering, a weak commensurate *solid* peak. The commensurate solid line shape is that discussed in Ref. 1 with a peak position $Q_{\text{comm}}=1.7003 \text{ \AA}^{-1}$ and a finite-size length of 1350 \AA . Over a temperature interval of ~ 0.5 K the commensurate intensity rises linearly while the fluid intensity decreases to zero. At no point do we observe a well correlated fluid as would be expected near a continuous transition. Thus the F-C transition is *first order*; we find similar behavior for the F-C transition at $T=124.5$ K, $P \approx 100$ Torr. This disagrees with the previous conclusions^{1,4,5} that the F-C transition is second order above 115 K. It should be noted that since our data represent scans in chemical potential, one would have expected a discontinuous jump in the commensurate intensity. We interpret the 0.5 K transition region as reflecting the inhomogeneity in the substrate binding energy. A similar broadening was reported previously in Ref. 1. Closely analogous behavior has recently been found for the F-C transition of N_2 on graphite.¹²

A saturated commensurate solid profile is observed at 127 K. Below ~ 126 K the peak intensity begins to decrease, signaling the reentrant melting transition. The data at 123.5 K show a weak commensurate solid peak together with the diffraction profile of a well-correlated weakly incommensurate fluid with $Q_0=1.713 \text{ \AA}^{-1}$ and $\kappa=0.009 \text{ \AA}^{-1}$. Again there is some smearing of the transition over a total range of ~ 0.5 K. The fits in the transition region are all somewhat unsatisfactory; however, for $T \leq 123.0$ K a single powder-averaged Lorentzian profile fits the data adequately. A representative fit for $T=122.25$ K is shown in Fig. 2. This reentrant C-RF transition thus appears to be continuous, in contrast to the upper C-F transition; however, because of substrate inhomogeneities we cannot rule out a small first-order jump at $T_c(\text{C-RF})$. The most important new qualitative feature of the RF data is that there is no evidence for the $-\epsilon/2$ superlattice peak ($\epsilon = Q_0 - Q_{\text{comm}}$) observed at lower temperatures.¹ Thus the modulated (or domain-wall) nature of this fluid is no longer evident.

The RF-IC and F-IC transitions at 310 and 600 Torr, respectively, are rather different from those observed previously in other systems^{8,13} in that the transitions are very gradual. The profiles are always well described by Lorentzians with the width gradually decreasing with decreasing temperature. In the IC solid phase the peaks may be described either by power-law singularities or by resolution-limited Lorentzians. Certainly, the freezing is continuous rather than strongly first order although the precise value of T_c is difficult to determine. In Fig. 1 we have plotted as T_c the temperature at which the HWHM equals that of the commensurate phase; this should be accurate to ± 1 K. As illustrated by the data at 116 K in Fig. 2, the power-law line shape expected for a floating solid,¹ $(Q - Q_0)^{\eta-2}$ with $\eta \sim 1/3$ near melting, describes the IC profile quite well. This, however, demonstrates consistency rather than uniqueness.

The parameters derived from fits to all of the scans at $P=310$ Torr and $P=600$ Torr are shown in Fig. 3. At 600 Torr there is a single F-IC transition. Both the peak posi-

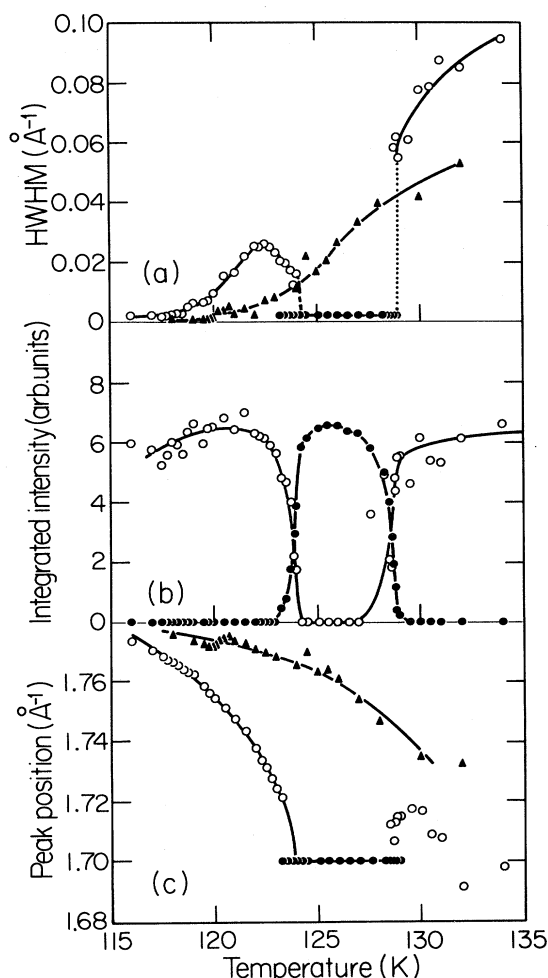


FIG. 3. Least-squares-fit parameters at $P=600$ Torr (triangles) and $P=310$ Torr (closed circles, commensurate; open circles, incommensurate). The peak position for $P=310$ Torr is a power law of $1/2$; the other lines are guides to the eye.

tion and the fitted peak width evolve smoothly through the presumed transition temperature of 122 K. Below 122 K, power-law singularities with $\eta \leq 1/3$ describe the data as well as Lorentzians. (The apparent feature in Q_{peak} at ~ 120 K is an artifact caused by a leak in the cryostat.) These experiments have thus demonstrated that 2D krypton exhibits a continuous F-IC solidification transition. The fluid correlation length however evolves much more gradually for 2D krypton than for xenon.¹³ Indeed, the behavior is closer to that of the 2D XY model.

As described above, the data at 310 Torr are much richer. As shown in Fig. 3, starting at 134 K the fluid inverse correlation length decreases continuously from ~ 0.1 to

$\sim 0.06 \text{ \AA}^{-1}$ and then jumps discontinuously to zero. This first-order character at these high temperatures disagrees with the lattice-gas theory of Ostlund and Berker;⁵ they predict a substrate-smeared second-order transition above ~ 80 K. Their theory nevertheless gives a very good description of the overall phase diagram in the submonolayer region. We believe that the essential features of their model are correct but that their predicted second-order transition is preempted by some other mechanism.

The C-RF transition is similar to that studied previously by Stephens and co-workers.¹ Specifically $\kappa \rightarrow 0$ as $\epsilon \rightarrow 0$ but with $\epsilon/\kappa \sim 1$ for $\epsilon \leq 0.04 \text{ \AA}^{-1}$; indeed, the region where $\epsilon/\kappa \sim 1$ is much more expanded at these higher temperatures.¹ There are, however, two significant differences from the lower-temperature results. First, no substrate modulation effects are evident in the profiles. Second, contrary to all the data below 94 K, where the incommensurability follows a universal curve^{1,2} with exponent $\sim 1/3$, we find that a power law with an exponent nearer $1/2$ is required. The solid line through the circles in Fig. 3(c) is a power law with $T_c = 123.9$ K and exponent 0.50. The reader should be cautioned, however, that if Huse and Fisher⁶ are correct and only data where κ is decreasing and ϵ/κ is constant should be included in the fits, then no meaningful exponents can be extracted from either these measurements or any previous experiments. Indeed, one unfortunate conclusion of this work is that a much higher quality substrate must be found before one will be able to determine the various exponents near T_c accurately enough to differentiate between the Huse-Fisher model and other theories.⁶

In this work we have shown that the modulated reentrant fluid separating the C and IC phases connects continuously onto the normal high-temperature fluid. A number of features of the monolayer krypton system, however, remain to be understood. These include the fact that the F-C transition is always strongly first order whereas the C-RF melting appears to be continuous. The very gradual nature of the F-IC or RF-IC transition is surprising in light of previous results for xenon on graphite¹³ and computer simulations.⁷ Finally, it would be very interesting to see if the domain-wall theories such as those discussed in Ref. 10 could be applied in sufficient detail to predict quantitatively our measured phase diagram and structure factors.

It is a pleasure to acknowledge stimulating discussions with A. N. Berker, M. Chan, and M. E. Fisher. We also thank the staff at SSRL for their kind assistance. The work at MIT was supported by the U.S. Army Research Office under Contract No. DAAG-29-81-0029 and by the National Science Foundation Materials Research Laboratory under Contract No. DMR-81-19295 and that at Brookhaven by the U.S. Department of Energy under Contract No. DE-AC02-76CH00016. One of us (M.S.) would like to acknowledge financial support from NATO, another (E.D.S.) financial support from The National Science Foundation.

¹R. J. Birgeneau, G. S. Brown, P. M. Horn, D. E. Moncton, and P. W. Stephens, *J. Phys. C* **14**, L49 (1981); D. E. Moncton, P. W. Stephens, R. J. Birgeneau, P. M. Horn, and G. S. Brown, *Phys. Rev. Lett.* **46**, 1533 (1981); P. W. Stephens, P. A. Heiney, R. J. Birgeneau, P. M. Horn, D. E. Moncton, and G. S. Brown, *Phys. Rev. B* **29**, 3512, (1984).

²M. D. Chinn and S. C. Fain, Jr., *Phys. Rev. Lett.* **39**, 146 (1977); S. C. Fain, Jr., M. D. Chinn, and R. D. Diehl, *Phys. Rev. B* **21**, 4170 (1980).

³D. M. Butler, J. A. Litzinger, and G. A. Stewart, *Phys. Rev. Lett.* **44**, 466 (1980).

⁴Y. Larher and A. Terlain, *J. Chem. Phys.* **72**, 1052 (1980).

- ⁵S. Ostlund and A. N. Berker, Phys. Rev. Lett. **42**, 843 (1979), and references therein.
- ⁶S. N. Coppersmith, D. S. Fisher, B. I. Halperin, P. A. Lee, and W. F. Brinkman, Phys. Rev. B **25**, 349 (1982); M. Kardar and A. N. Berker, Phys. Rev. Lett. **48**, 1552 (1982); D. A. Huse and M. E. Fisher, *ibid.* **49**, 793 (1982).
- ⁷F. F. Abraham, W. E. Rudge, D. J. Auerbach, and S. W. Koch, Phys. Rev. Lett. **52**, 445 (1984), and references therein.
- ⁸M. Nielsen, J. Als-Nielsen, J. Bohr, and J. P. McTague, Phys. Rev. Lett. **47**, 582 (1981); Phys. Rev. B **25**, 7765 (1982).
- ⁹D. E. Moncton and G. S. Brown, Nucl. Instrum. Methods **208**, 579 (1983).
- ¹⁰R. Caflisch, M. Kardar, and A. N. Berker (unpublished).
- ¹¹J. G. Dash and R. T. Muirhead (unpublished).
- ¹²K. D. Miner, Jr., M. W. H. Chan, and A. D. Migone, Phys. Rev. Lett. **51**, 1465 (1983).
- ¹³P. A. Heiney, P. W. Stephens, R. J. Birgeneau, P. M. Horn, and D. E. Moncton, Phys. Rev. B **28**, 6414 (1983).